Influence of Brittle Property of Cement Treated Soil on Undrained Bearing Capacity Characteristics of the Ground

S. Yamada[1], T. Noda[2], A. Asaoka[3] and T. Shiina[4]
[1]*Department of Civil Engineering, Nagoya University, Nagoya, Japan*
[2]*Disaster Management office, Nagoya University, Nagoya, Japan*
[3]*Association for the Development of Earthquake Prediction, Tokyo, Japan*
[4]*Former Institute of Technology, Penta-Ocean Construction Co., Ltd., Tochigi, Japan*
E-mail: s-yamada@civil.nagoya-u.ac.jp

ABSTRACT: In this study, the influence of brittle property of geomaterials on the failure behavior of the ground in an undrained bearing capacity problem was investigated numerically from the standpoint of taking the brittle behavior of cement treated soil as softening behavior of the soil element. The numerical analyses were performed using the soil-water coupled finite deformation analysis code ***GEOASIA*** mounted with the SYS Cam-clay model, which describes the soil skeleton structure at work. Cement treated ground and naturally deposited clay ground were modelled and compared, and it was found that they showed widely differing failure processes depending on differing initial conditions. Especially, it was found that when progressive failure in which strain localization region develops due to propagation of material failure occurs, even though the ground is composed of brittle materials such as cement treated soil, those brittle properties do not directly manifest in the load-settlement relationship. Additionally, the investigation revealed that, since every soil element on the slip lines does not reach its peak strength simultaneously when progressive failure occurs, post-peak material properties, i.e. the ratio of residual strength to peak strength and softening rate from peak to residual state, affect the bearing capacity of the ground.

1. INTRODUCTION

Cement stabilization has become one of the most essential techniques for ground improvement in geotechnical engineering. Sea reclamation projects using pneumatic flow mixing method, which is one of the ground improvement techniques by cement stabilization, has increased in recent years, of which a typical example is the Central Japan International Airport. In this method, a hardener is added to pneumatically transported slurry while it is inside the pipe, and the turbulent flow effect caused by the resulting plug flow agitates and mixes the slurry and hardener. Land reclaimed using this method has some advantages: (1) The method allows the use of large volumes of dredging slurry, which is difficult to handle due to its high water content; and (2) the land becomes usable a shorter time after the reclamation project is completed. However, this kind of cement treated soil still holds a high water content after hardening, and its design strength is usually 100 – 200 kN/m^2 (Coastal development institute of technology 2008). Therefore, it is lower in strength and has a higher latent compressibility than soil prepared by deep mixing or other cement treated methods. Therefore, civil engineers must exercise caution with respect to soil stability and settlement when constructing structures on reclaimed land. The issue in cement treated soil that crops up most often in investigations of stability is its brittle property. Cement treated soil specimens demonstrate their peak strength at low strain level, and then show sharp losses in strength. There is concern that when the ground consists of soil with these material properties, once failure has been initiated, it progresses sharply through stress redistribution and can lead to catastrophic collapse.

Yamamoto et al. (2004) studied on the bearing capacity of cement treated ground the strength of which is comparatively lower. In that study, the model experiments of the ground improved by fly ash gypsum cement deep mixing method and the numerical simulations by finite difference method using elasto-perfect plastic model following the Mohr-Coulomb yield criterion were carried out. Kasama et al. (2012) conducted reliability analysis on the bearing capacity of cement-treated ground considering the spatial variability of shear strength based on Monte-Carlo simulations using the random field numerical limit analyses. Although both of these studies presented important knowledge, they did not treat the progressive failure as well as most of the previous numerical studies on cement treated ground. On the other hand, for the concern mentioned above, we investigated the influence of the brittle property of geomaterials on the failure behavior of the grounds by means of a soil-water coupled finite deformation analysis mounted with an elasto-plastic constitutive equation, taking an undrained bearing capacity problem as an example. Specifically, we considered that cement treated soils were pseudo-overconsolidated soils (Tashiro et al. 2004) given structure artificially, and then described brittle behavior shown by cement treated soils as softening behavior at a material level using the SYS Cam-clay model (Asaoka et al. 2002), which is an elasto-plastic constitutive equation of geomaterial incorporating the work of the soil skeleton structure (structure, overconsolidation, anisotropy). Additionally, the soil-water coupled finite deformation analysis code ***GEOASIA*** (Asaoka et al. 1994; Noda et al. 2008) with the constitutive equation was also used to solve the initial-boundary value problems for cement treated ground. As a result of the numerical simulation, progressive failure, which previous studies could not recreate, is shown. By comparing with an undrained bearing capacity analysis of naturally deposited clay ground, which is previous analysis using the same analysis code (Noda et al. 2007a), it is demonstrated that the brittle property may not be directly reflected or they may be strikingly reflected in the bearing capacity characteristics of the ground in accordance with differing failure process.

Also, the concern mentioned above has been the main motivation for one of the recent booms in research into improving the brittle property of cement treated soils. For example, Tsukiji et al. (1998) mixed plastic wastes into cement treated soils and Mitarai et al. (2007) mixed tire chips; both groups showed that these trials changed the brittle material into the ductility material. However, it is still not well understood that what significance these trials to improve post-peak material properties actually hold for stability problems of ground. This paper presents a systematic study of the effect that the improvement of brittle property at a material level had on the bearing capacity of the ground, using the above analysis code.

2. SIMULATION OF THE MECHANICAL BEHAVIOR OF CEMENT TREATED SOIL USING THE SYS CAM-CLAY MODEL

This chapter provides the results of undrained triaxial shear tests on cement treated soil. From the standpoint that triaxial shear test is taken as an element test, the brittle failure behavior shown by the cement treated soil is attempted to reproduce using SYS Cam-clay model, which is an elasto-plastic constitutive equation incorporating the soil skeleton structure at work, as softening behavior at an element level.

2.1 Undrained Triaxial Shear Behavior in Cement Treated Soil

The physical properties of the raw material soil that was the subject of improvement and the cement blending conditions are shown in Table 1. The soil dredged from a port in Japan was used as the raw material soil. The target strength in the unconfined compression test at 28 days was set to 200kPa. Also, the initial water content was set to 1.8 times the liquid limit in order to obtain good fluidity during construction. The hardener was blast-furnace slag cement type B. The parameters shown in Table 1 were chosen in order to satisfy the above conditions.

A triaxial shear test was carried out on the cement treated soil specimens made as described above. The tests were conducted without capping, because the specimens were relatively soft for cement treated soil. The confining pressure was set to 50kPa or 200kPa and then an undrained shear test was performed; Figure 1 presents the results. Under a confining pressure of 50 kPa, hardening accompanied by an increase in the mean effective stress *p'* (plastic expansion) first occurred, followed by softening accompanied by a decrease in the mean effective stress *p'* (plastic compression). It can also be seen that under a confining pressure of 200kPa, softening occurred with a decrease in the mean effective stress p' (plastic compression). This bears a close resemblance to the behavior observed in naturally deposited clay (Nakano et al. 2005) (Figure 2), but cement treated soils reach their peak strength at lower levels of strain than typical naturally deposited clays, and then show abrupt softening.

Table 1 Properties and blending conditions of the raw material soil

[Physical properties]		
Soil particle density ρ_s (g/cm^3)		2.70
Liquid and plastic limits	Liquid limit *LL* (%)	82.0
	Plastic limit *PL* (%)	34.0
	Plasticity index *PI*	48.0
Grain size distribution and plasticity	Sand content (%)	2.0
	Silt content (%)	48.0
	Clay content (%)	50.0
[Blending conditions]		
Water content of the blended soil w_0 (%)		147.0
Quantity of cement added *C* (kg/m^3)		65.5

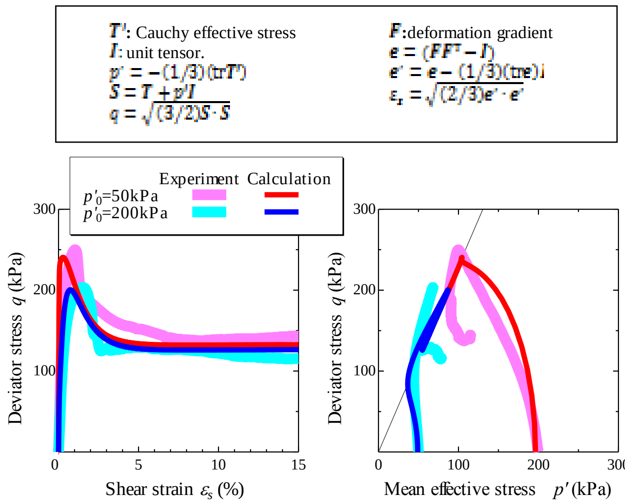

Figure 1 Undrained shear behaviours of cement treated soil and its reproduction by SYS Cam-clay model

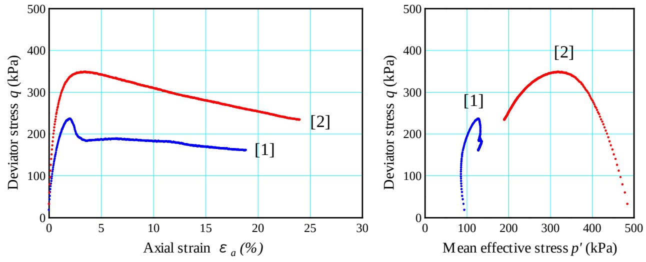

Figure 2 Undrained shear behaviors of naturally deposited clay (after Nakano et al. 2005)

2.2 Reproduction of Undrained Triaxial Shear Behavior in Cement Treated Soil Using the SYS Cam-clay Model

The SYS Cam-clay model was used to attempt to reproduce the undrained triaxial shear behavior seen in Figure 1. The values given in Table 2 for the material constants and initial values were employed here (the symbols used in Table 2 have been explained in previous papers describing the SYS Cam-clay model (Asaoka et al. 2002; Noda et al. 2007b)). In determining these values, it was considered that the soil was artificially given structure by the addition of the hardener, so the initial structure $1/R^*$ was given. Here, "structure" is a concept that gives soils the bulk characteristics, as typified the card house like structure of naturally deposited clay. The overconsolidation ratio $1/R$ was calculated using the other initial values in Table 2 (Noda et al, 2005). The fact that this value is greater than 1 with no particular stress history indicates that the cement treated soil is in a pseudo-overconsolidated state (Tashiro et al. 2004). In general, initial anisotropy is considered to develop during depositional process, i.e. one dimensional self-weight consolidation process. On the other hand, cement treated soil does not undergo such as one dimensional compression process because it becomes stiff before the occurrence of self-weight consolidation. That is to say, it was assumed that plastic deformation that would cause anisotropy has not occurred, so it was initially assumed that the state was isotropic. When overconsolidated soil with a developed structure is subjected to plastic deformation, the structure is degraded and the overconsolidation is relieved; ultimately, the soil approach asymptotically to remolded and normally consolidated state. The changes in structure, overconsolidation and anisotropy during this process are described by the evolution laws for R^*, R and $\boldsymbol{\beta}$ (In regard to the evolution rule for R^*, the method of using the norm of the shear component $\|\boldsymbol{D}_s^p\|$ and the volumetric component D_v^p of the plastic stretching (Noda et al. 2007b) was used.). The degradation index of structure *a*, which is an evolution parameter for R^*, is the value which determines the rate per unit of plastic deformation at which the card house structure collapses. The concrete values of material constants, which includes *a*, and initial values were decided by curve fitting method for the triaxial test results. Table 2 indicates that this value is considerably larger than the material constant estimated for naturally deposited clay (Table 3), which will be explained later, but this reflects the brittle property of cement treated soil. The initial values presented in Table 2 are those for a confining pressure of 50kPa. Simulation of the undrained triaxial shear test under a confining pressure of 200kPa was carried out, incorporating the process of isotropic compression from this condition.

Figure 1 presents the calculation results of the SYS Cam-clay model along with the actual experimental results. Under the pre-determined conditions described above (Table 2), the SYS Cam-clay model generally reproduced the previously described behavior for cement treated soil. The predicted ratio between the peak strength and residual strength is also quite consistent with the experimentally observed value. Of course, the post-peak behavior of experimental results is affected by strain localization. On the other hand, in the above simulation using SYS Cam-clay model, the softening behaviour was treated as an element behavior. In the following sections, we studied on the effects of brittle properties on boundary value problems from the macro perspective to treat brittle behavior shown by cement treated soil as softening behavior of the element.

Table 2 Material constants and initial values (cement treated soil)

[Elasto-plastic parameters]	
Compression index $\tilde{\lambda}$	0.9
Swelling index $\tilde{\kappa}$	0.004
Critical state constant M	2.3
Specific volume at q = 0 and p' = 98.1kPa on NCL N	5.45
Poisson's ratio ν	0.15
[Evolution rule parameters]	
Degradation index of structure a (b, c)	8.0 (1.0, 1.0)
c_s	0.9
Degradation index of overconsolidation m	9.0
Evolution index of rotational hardening b_r	0.01
Limit of rotational hardening m_b	0.6
[Initial values]	
Specific volume v_0	5.36
Overconsolidation ratio $1/R_0$	6.66
Degree of structure R^*_0	0.333
Mean effective stress p'_0 (kPa)	50.0
Lateral pressure coefficient K_0	1.0
Degree of anisotropy ζ_0	0.0
Permeability coefficient k (cm/sec)	1.0×10^{-6}
Density of soil particle ρ_s (g/cm^3)	2.70

3. UNDRAINED BEARING CAPACITY OF CEMENT TREATED SOIL

Next, the material constants and initial values (Table 2) employed to reproduce the undrained triaxial shear test with cement treated soil were used to examine the undrained bearing capacity characteristics of cement treated ground with the analysis code ***GEOASIA***. Here, an example of the undrained bearing capacity analysis of a naturally deposited clay ground (Noda et al. 2007a) was selected from among past research using the same analysis code, and the forms of failure progression in it and the present cement treated ground are compared with each other and discussed.

3.1 Analytical conditions

The calculations were carried out under plane strain conditions. Figure 3 shows the finite element mesh and boundary conditions. A typical bearing capacity problem was considered, so the problem was set as a vertical displacement applied to a rigid frictional foundation. For simplicity, linear constraint conditions (Asaoka et al. 1998) (conditions with the distances and angles constant) were applied between the nodes corresponding to the foundation. Analysis was carried out for the whole cross-section, but the analysis conditions did not allow for inclination or slippage of the foundation. This was because if a non-symmetrical deformation mode appeared, the load reduction would be more significant than the case of symmetrical deformation (Noda et al. 2007a), but nonetheless, the aim was to indicate the extent of load reduction in the absence of this effect. The vertical displacement was applied to the central node of the foundation at a high speed (10^{-3}cm/sec) so that there would be virtually no migration of pore water within the ground.

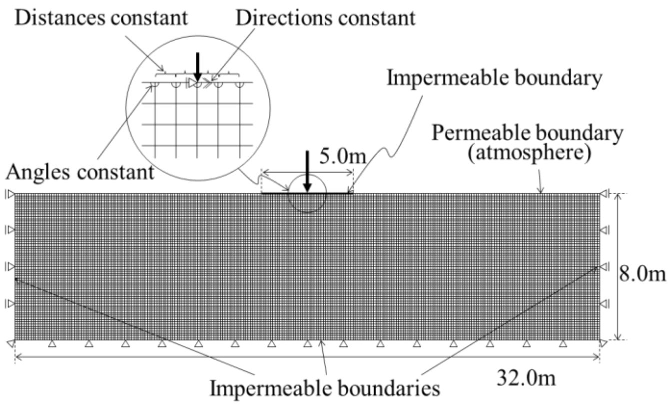

Figure 3 Finite element mesh and boundary conditions

3.2 Results of Undrained Bearing Capacity Analysis of Cement Treated Soil

Here, the results of the analysis of the undrained bearing capacity of cement treated ground are presented, under the assumption that the reclaimed soil was formed by pneumatic flow mixing or a similar process. The values shown in Table 2 were used as the material constants necessary for the SYS Cam-clay model. The initial conditions were determined as follows based on Table 2 and taking self-weight into consideration. Normally when an area is reclaimed using cement treated soil, hardening of the ground proceeds at a rate that is much faster than the rate of consolidation due to self-weight, even when the original soil has a fairly high water content. After hardening, the excess pore water pressure dissipates, and even though the effective stress increases, the ground has literally hardened by that time, so there is almost no reduction in the void ratio. This means that if non-uniformity associated with inadequate mixing is ignored, a ground with a uniformly high water content will be formed in the depth direction. Also, if it is likewise assumed that the cement has been uniformly mixed throughout the whole ground, the initial value of the quantitative index $1/R^*$ that expresses the degree of the structure is constant throughout the ground. Additionally, since the hardening speed of cement treated soil exceeds the speed of self-weight consolidation, dissipation of excess pore water pressure leads to little compression. Therefore, it was assumed that the initial anisotropy was not developed and the initial stress state was isotropic. The specific values used were the same as those shown in Table 2, apart from the overconsolidation ratio $1/R$. Under these conditions, the initial stress and initial overconsolidation ratio were calculated taking self-weight into consideration with a very small load (9.81×10^{-2} kPa) acting vertically on the surface. The load applied to the surface was a small value such that the initial distributions were virtually unchanged even if the value was reduced by one order of magnitude. Fig. 4 shows the initial distributions in the ground. The calculated overconsolidation ratio (Noda et al. 2005) became smaller the greater the depth. This corresponds to the fact that the vertical effective stress increases with depth of the ground, whereas the consolidation yield stress of a cement treated ground is virtually constant with depth. Also, the undrained shear "strength" q_u shown in Figure 4 represents the unconfined compression strength of clay material (Noda et al. 2005) obtained by numerically reproducing an ideal sampling state. The "strength" of the ground is virtually constant in the depth direction, reflecting the assumption that the cement has been uniformly mixed.

The analysis of the undrained bearing capacity of cement treated ground is now considered. Figure 5 shows the load-settlement relationship (the vertical load means the total reaction force from the ground acting on the foundation, divided by the foundation surface area) and Figure 6 shows the shear strain distributions. From the shear strain distributions, it can be seen that initially, strain localization occurred directly under the edges of the foundation, and subsequently, the strain localization region propagated and ultimately formed slip lines in the shape of a circular arc. In this manner, failure in reclaimed ground treated with cement takes the form of progressive failure. However, although clear strain localization occurs shown in Figure 6, there is no distinct load reduction in the load-settlement relationship shown in Figure 5, contrary to what would be expected from the brittle behavior at the material level.

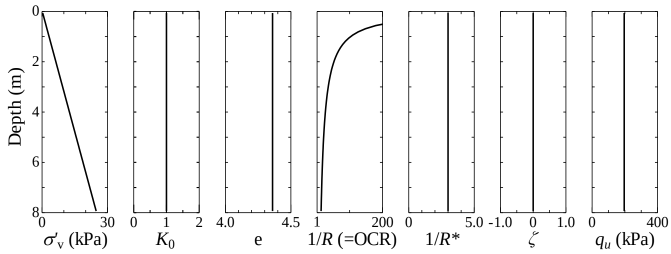

Figure 4 Initial distributions of state variables
(cement treated ground)

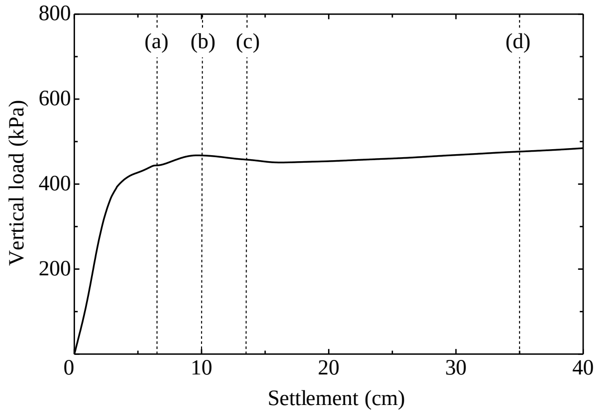

Figure 5 Relation between load and settlement
(cement treated ground)

3.3 Comparison with an Undrained Bearing Capacity Analysis Result of Naturally Deposited Clay Ground

Here, a result of undrained bearing capacity analysis of a naturally deposited clay ground (Noda et al. 2007a) was selected among past research using the same analysis code for comparison. The material constants and initial values shown in Table 3 were used for this calculation (the method (Asaoka et al. 2002) of using the norm of plastic stretching $\|\boldsymbol{D}^p\|$ was used for the evolution law for R^*). The material constants were selected to reproduce the elasto-plastic behavior typical for clay (overconsolidation is relieved faster than structural degradation; development of anisotropy is slow). The value of a = 0.2 for the structural degradation index here is considerably lower than a = 8.0 in Table 2 for cement treated soil, which illustrates that this is a relatively ductile soil. In contrast to the method used in the simulation of cement treated soil, after the surface load (98.1 kPa) was removed from normally consolidated soil which had initially developed structure and anisotropy, consolidation calculations were conducted until the excess pore water pressure had completely dissipated. The bearing capacity analysis was carried out on this substantively overconsolidated ground where the above surface load was removed. The reason of the unloading process at the ground surface is usually related to the erosion of upper layer after crustal movement, glacier melt or artificial loading history etc. In Figure 7, OCR is around 1.0 despite the ground has been subjected to unloading history and K_0 is more than 1.0. It is because that the soil ground underwent loading history in the triaxial extension side in plastic mechanics as a result of removing of the surface load (see Noda et al. (2007) for details on initial treatment of the ground and the characteristics of the ground created in this way). Figure 7 shows the initial distributions of several soil parameters.

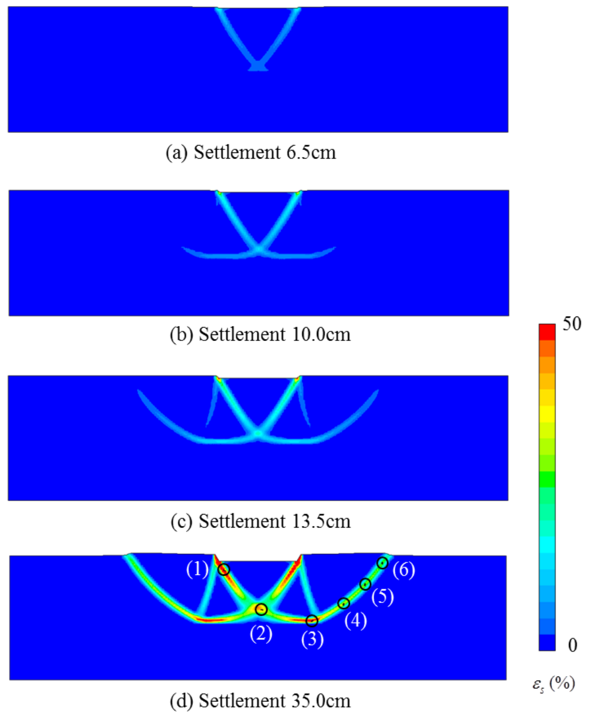

(a) Settlement 6.5cm
(b) Settlement 10.0cm
(c) Settlement 13.5cm
(d) Settlement 35.0cm

Figure 6 Shear strain distributions
(cement treated ground)

Table 3 Material constants and initial values
(naturally deposited clay ground)

[Elasto-plastic parameters]	
Compression index $\tilde{\lambda}$	0.23
Swelling index $\tilde{\kappa}$	0.01
Critical state constant M	1.15
Specific volume at q = 0 and p' = 98.1kPa on NCL N	2.75
Poisson's ratio ν	0.1
[Evolution rule parameters]	
Degradation index of structure a (b, c)	0.2 (1.0, 1.0)
c_s	5.0
Degradation index of overconsolidation m	0.001
Evolution index of rotational hardening b_r	1.0
Limit of rotational hardening m_b	0.23
[Initial values]	
Overconsolidation ratio $1/R_0$	1.0
Degree of structure $1/R^*_0$	4.0
Lateral pressure coefficient K_0	0.5
Degree of anisotropy ζ_0	0.75
Permeability coefficient k (cm/sec)	2.8x10^{-7}
Density of soil particle ρ_s (g/cm^3)	2.75

Figure 8 shows the load-settlement relationship and Figure 9 shows the shear strain distributions. The fact that there is clear strain localization in the shape of circular arcs is also consistent with the cement treated ground. However, even though this soil was relatively ductile, the load reduction in the load-settlement relationship is more significant in Figure 8, representing naturally deposited clay ground, than that in Figure 5, representing cement treated ground. As can be seen from these examples, the material property may not be reflected, or they may be reflected in the solution of an initial-boundary value problem in accordance with differences in such things as material constants and initial conditions of the ground. What brings about these differences?

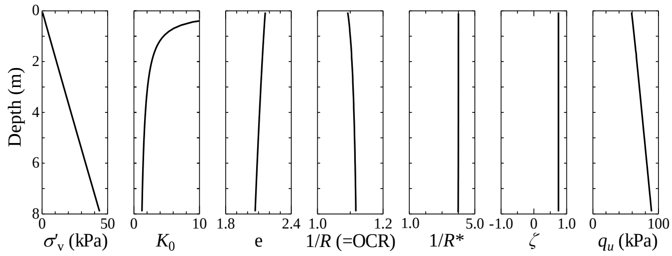

Figure 7 Initial distributions of state variables (naturally deposited clay ground)

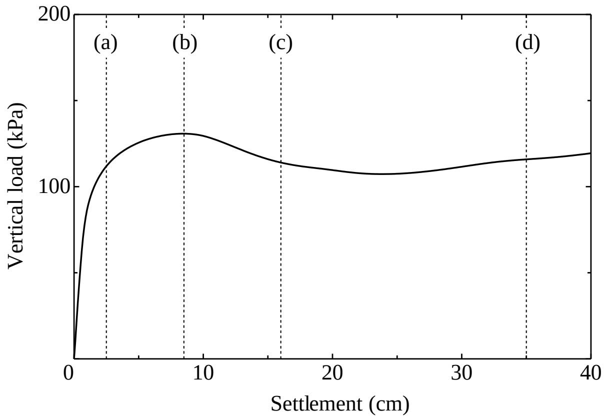

Figure 8 Relation between load and settlement (naturally deposited clay ground)

The behavior of each element in the strain localization region within the ground is considered in a search for answers to the above question. Figures 10 and Figure 11 show the behavior of the elements on the slip lines of cement treated soil and naturally deposited clay (the locations of the elements are shown in the distributions in Figure 6(d) and Figure 9(d)). The points plotted as (a) through (d) for the behavior of each element in Figure 10 and Figure 11 represent the states at times (a) through (d) shown for the load-settlement relationship of the grounds (Figure 5 and Figure 8). Comparing the behaviors of the two grounds, it can be seen that each of the elements of Figure 10 show sudden softening compared with each of the elements in Figure 11, clearly showing the brittle behavior of the cement treated soil at the element level.

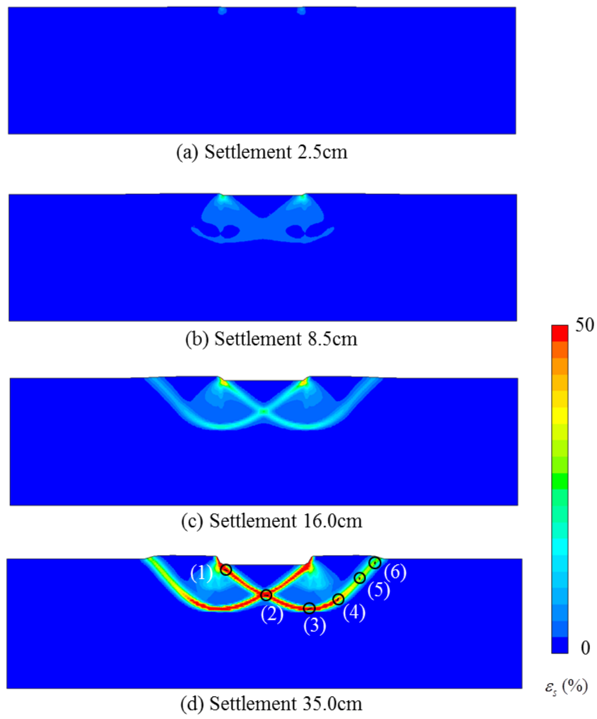

Figure 9 Shear strain distributions (naturally deposited clay ground)

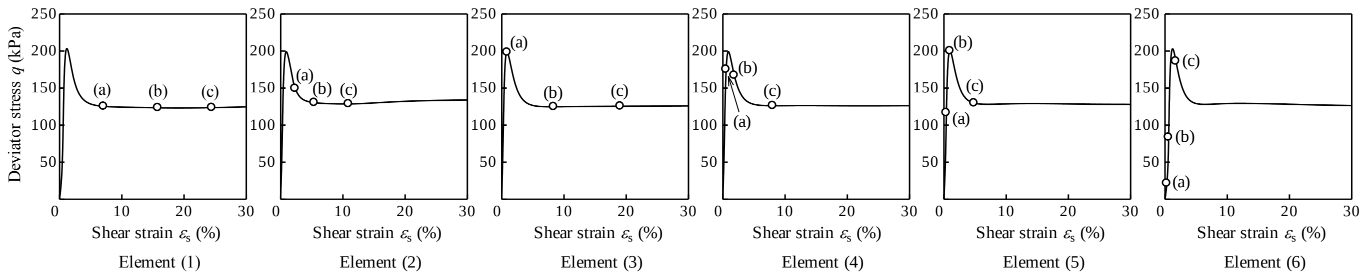

Figure 10 Element behaviors on the slip line (cement treated ground)

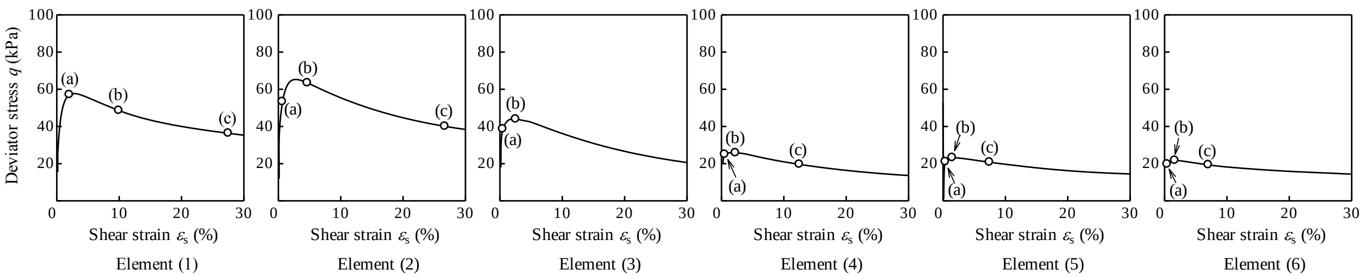

Figure 11 Element behaviors on the slip line (naturally deposited clay ground)

In addition, there are various other differences between the two grounds, but what is particularly significant is the difference in the timing of the peaks of each element. In the cement treated ground, although there are elements that start to soften before the appearance of the peak in the load-settlement relationship, there are also elements that start to soften after the appearance of the peak. In contrast, in the naturally deposited clay ground, all the elements except element (1) directly under the edge of the foundation start to soften at virtually the same time as appearance of the peak in the load-settlement relationship. Looking at this in a little more detail, in the cement treated ground, softening occurred sequentially from element (1) to element (6), i.e., directly under the edge of the foundation towards the other end of the slip line. In contrast, in the naturally deposited clay ground, softening is produced at the same time as if waiting for all the elements to reach their peaks. This difference faithfully represents the method of progression of strain localization. In the shear strain distributions for the cement treated ground shown in Figure 6, it can be seen that the slip lines extend gradually from the edges of the foundation. Moreover, localization has already progressed before arrival at the peak, a temporary wedge is formed around the peak, and then circular arc slip lines is finally formed. In contrast, in the naturally deposited clay ground shown in Figure 9, strain localization proceeds all at once after the peak, forming a circular arc slip line, and then the slip lines becomes clear as the foundation presses down. Of course, the difference in the manners in which load reduction occurs in the two grounds, which can be seen in the load-settlement relationship, is caused by the differences in the process of progression of failure: whether softening occurs gradually at the element level, or whether softening occurs all at once. Also, based on the point of view that strain localization region develops due to the propagation of material failure at the element level, it is appropriate to call the failure of the reclaimed ground treated with cement as conceived above in section **3.2** "progressive failure".

Although the following discussion diverges slightly from the main topic of this paper, we want to point out an additional aspect besides the above disparities between cement treated ground and naturally deposited clay ground. While the peak strength of the elements of cement treated ground is about 200kPa in all locations, the elements of naturally deposited clay display a wide range of strengths. One of the factors suggested as giving rise to this disparity is that the void ratio in cement treated ground is constant throughout the ground, while in naturally deposited clay, it decreases with increasing depth. However, an even more significant factor is that the cement treated ground is initially in isotropic state, whereas naturally deposited clay ground is initially in anisotropic state. There have been many discussions of the influence of anisotropy on the bearing capacity of grounds composed of geomaterials that can display softening behavior as well as the influence of progressive failure (Oda et al, 1979; Tatsuoka 1992, 2007). Most of previous descriptions of the influence of anisotropy have been discussed comparing the slip line of a bearing capacity problem with the orientations of the shear bands observed in various laboratory element tests. Those papers typically speculate that each element on the slip lines of the bearing capacity problem is supposed to display different peak strength, since different peak strengths were obtained by changing the orientation of the principal stress planes and the bedding planes when using anisotropic specimens in element tests (Oda et al. 1978). The difference in the peak strength of the each element in Figure 11 actually demonstrates the effect of anisotropy on bearing capacity, which has been speculated by researchers and engineers based on the element test results.

3.4 Effects of initial conditions on failure process of ground

The above discussion has demonstrated that the material property may not be directly reflected or they may be strikingly reflected in the solution of an initial-boundary value problem. It was also shown that this was due to the differing failure processes. This section continues the discussion and investigates which distinctions among the conditions in the two grounds are the main causes of the differences in the failure processes.

Next, while the material constants of the cement treated ground were applied, the initial conditions were given with the identical method used in the simulating naturally deposited clay ground. The initial values used before the load was removed from the ground surface were the level of structure $1/R^*_0$, the coefficient of earth pressure at rest K_0, the level of anisotropy ζ_0, as given in Table 2. The initial overconsolidation ratio $1/R_0$ was set to 1.0, as in the naturally deposited clay ground, i.e., normal consolidation state. The ground was changed into substantively overconsolidated state by removing the load from the ground surface. Figure 12 shows the initial distributions of soil parameters in this virtual ground (Since the state of most cement treated ground is not in the state mentioned above, we call the ground assumed in this section "virtual ground".).

Figure 13 shows the load-settlement relationship and Figure 14 shows the shear strain distributions. From the shear strain distributions, it can be seen that just as slip lines for the naturally deposited clay ground in Figure 9, circular slip lines appear abruptly in this virtual ground after the peak load; subsequently, strain localization level increases with continued penetration. In Figure 13, it can be seen that there is a greater load reduction than the load-settlement relationship for cement treated ground in Figure 5. Figure 15 presents the behavior of soil elements on the slip line (the location of each element is shown in Figure 14(d). The points plotted as (a) through (d) for the behavior of each element in Figure 15 represent the states at times (a) through (d) shown for the load-settlement relationship of the grounds (Figure 13). As expected, nearly all the soil elements of this virtual ground reached a peak simultaneously, as seen in the naturally deposited clay shown in Figure 11. The peak load in Figure 13 appears at a lower settlement than in Figure 5 and Figure 8 (it should be noted that the horizontal scales in Figure 13, Figure 5 and Figure 8 are different).

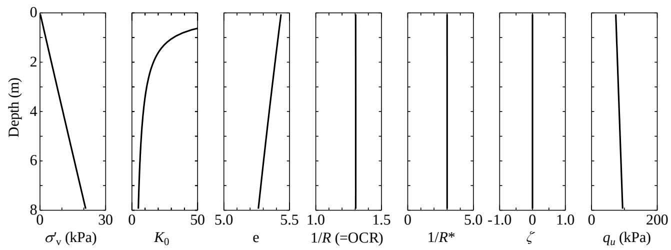

Figure 12 Initial distributions of state variables
(virtual ground, which has the material constants of the cement treated ground, and of which the initial conditions were given with the identical method used in the simulating naturally deposited clay ground)

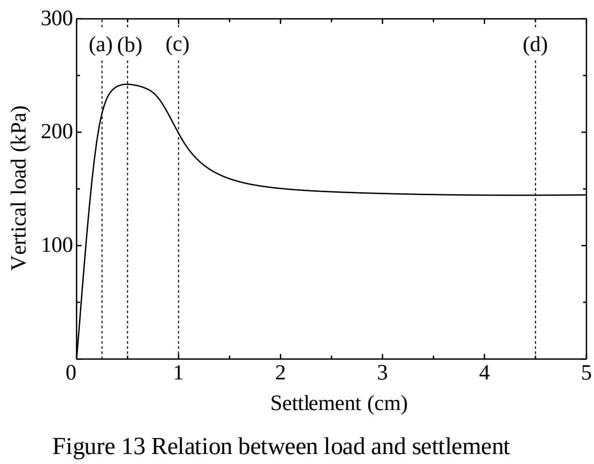

Figure 13 Relation between load and settlement
(virtual ground)

The slip lines in Figure 14 reach all the way to the ground surface while the strain is at an extremely low level (note that the maximum scale values in Figure 14, Figure 6 and Figure 9 differ). As mentioned above in section 2, cement treated ground reaches its peak strength at a low level of strain (see Figure 1). Thus, we can say that these characteristics are consequences from the material properties. As these analytical results provides, even though two grounds consist of the geomaterials with identical properties, if their initial conditions are different, great differences can appear in their failure process. Therefore, if cement treated ground was created in the condition shown in Figure 12, the ground would display the extremely brittle failure described in this section.

(a) Settlement 0.25cm

(b) Settlement 0.5cm

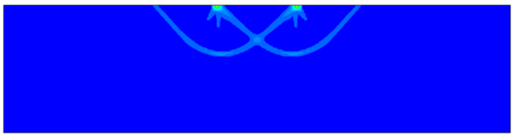

(c) Settlement 1.0cm

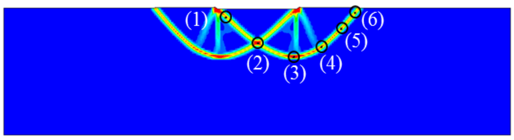

(d) Settlement 4.5cm

Figure 14 Shear strain distributions (virtual ground)

4. INFLUENCE OF BRITTLE PROPERTIES OF GEOMATERIALS ON UNDRAINED BEARING CAPACITY CHARACTERISTICS

The above discussion has demonstrated that when the initial conditions in Figure 4 are valid in ground that has been treated with cement, the slip lines develop gradually from the edges of the foundation in progressive failure mode, caused by the propagation of material failure at the element level. It is now clear that when this progressive failure occurs, the consequences of the material properties tend not to directly manifest themselves in the results of boundary value problems. On the basis of this finding, next, the influence of the brittle properties of geomaterial on the undrained bearing capacity was systematically examined, focusing on progressive failure.

In this section, the ratio of residual strength to peak strength and the softening rate from peak to residual state in undrained triaxial shear are taken as factors responsible for the brittle property of the soil, and these factors are examined for their influence on the undrained bearing capacity. Here, the "softening rate" refers to the rate at which softening proceeds per unit of plastic deformation, and is not a time-based rate.

4.1 Influence of the Ratio of Residual Strength to Peak Strength of Geomaterials

Let us begin with the influence of the ratio of residual strength to peak strength of the geomaterials on the bearing capacity. Three geomaterials with equal peak strengths but differing residual strengths under the conditions of undrained triaxial shear test were defined here, using some of the material constants and initial values for cement treated soil in Table 2. Table 4 shows the main material constants and initial values used for this discussion. Values other than those given in Table 4 are equal to those given in Table 2. Also, Case A2 had exactly the same conditions as in the analysis of cement treated ground examined in section **3**, and this was used as the baseline. The degradation index of structure *a* was constant in all cases in order to compare them with approximately equal softening rates from peak to residual state. In order to uniquely identify the residual strength using the specific volume v in the SYS Cam-clay model, v was set to values corresponding to progressively lower residual strengths in the order Cases A1 to A3, and the degree of development of the structure $1/R^*$ was set to provide equal peak strengths. The overconsolidation ratio $1/R$ was calculated using those values.

Figure 16 shows the undrained shear behavior in each case. It can be seen that the peak strength was equal in all cases and that the residual strength was lower in the order A1, A2, A3; the ratios of residual strength to peak strength were 0.75, 0.63 and 0.50, respectively.

Figure 17 presents load-settlement relationships, and Figure 18 presents the shear strain distributions for grounds composed of these materials. It is plain from the curves in Figure 17 that even when the peak strengths were equal at the material level, when the residual strengths differ, differences showed up in the bearing capacity (peak load) of the ground. To be more specific, the lower the ratio of residual strength to peak strength, the smaller the bearing capacity of the ground. The reason the residual strength affects the peak strength in these cases is that the elements on the slip lines reach their peak strengths at different times. In other words, as can be seen in Figure 10, when the load-settlement relationships of the ground reaches its peak, part of the elements on the slip lines have already reached the residual state or are in the softening state when the peak appears on the load-settlement relationship.; this is how the residual strengths affect the bearing capacity (peak load). It can be seen in the shear strain distributions in Figure 18 that the lower the ratio of residual strength to peak strength of a material, the more abrupt its localization is. Also, the slip lines approach the shape of a circular arc in ground as the residual strength is low, i.e., the ratio of residual strength to peak strength affects the shape of the failure mode.

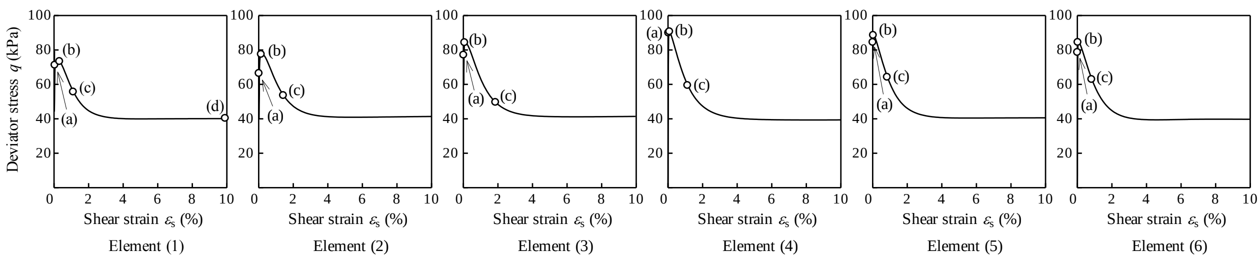

Figure 15 Element behaviors on the slip line (virtual ground)

Table 4 Main material constants and initial values
(influence of the ratio of residual strength to peak strength)

	Case A1	Case A2	Case A3
[Evolution rule parameter] Degradation index of structure a	8.0	8.0	8.0
[Initial values]			
Specific volume v_0	5.21	5.36	5.56
Overconsolidation ratio $1/R_0$	6.24	6.66	7.01
Degree of structure $1/R^*_0$	2.38	3.00	3.95

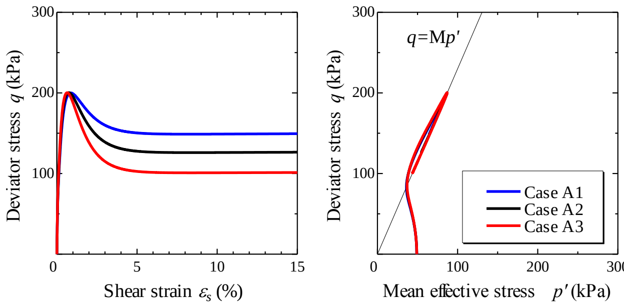

Figure 16 Undrained shear behaviors
(influence of the softening rate from peak to residual state)

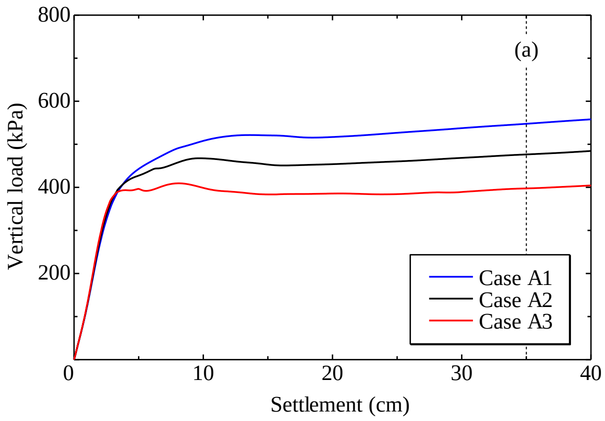

Figure 17 Relation between load and settlement
(influence of the ratio of residual strength to peak strength)

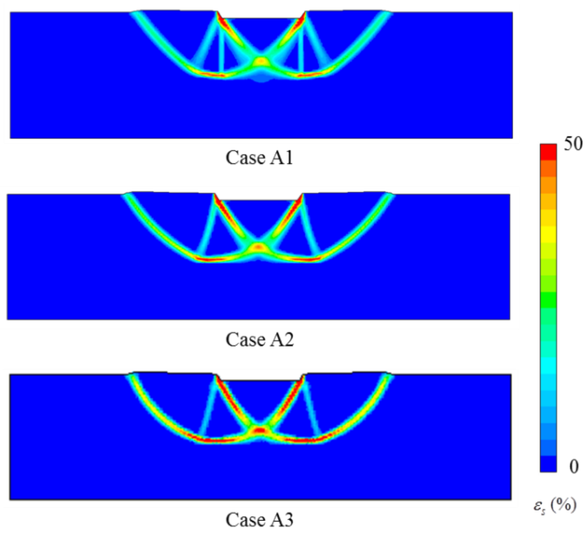

(a) Settlement 35.0cm

Figure 18 Shear strain distributions
(influence of the ratio of residual strength to peak strength)

4.2 Influence of Softening Rate from Peak to Residual State

Let us turn to the influence of the softening rate from peak to residual state on bearing capacity characteristics. Three softening rates were analyzed here. Table 5 shows the material constants and the initial values which are keys to this discussion. As in section **4.1** above, the values not shown in Table 5 were identical to those given previously in Table 2. Case B2 employed conditions identical to the cement treated ground analyzed previously in section **3**, and this was used as the baseline, as in the immediately preceding section. The degradation index of structure a was set so that the softening rate increased in the order of cases B1, B2, B3. Meanwhile, v was set so that the residual strength was equal in all cases, and $1/R^*$ was set so that the peak strength was equal. The overconsolidation ratio $1/R$ was calculated from the above values.

Table 5 Main material constants and initial values
(influence of the softening rate from peak to residual state)

	Case B1	Case B2	Case B3
[Evolution rule parameter] Degradation index of structure a	4.0	8.0	16.0
[Initial values]			
Specific volume v_0	5.36	5.36	5.36
Overconsolidation ratio $1/R_0$	5.19	6.66	9.32
Degree of structure $1/R^*_0$	2.34	3.00	4.20

Figure 19 shows the undrained shear behavior in all of these cases. It can be seen that the peak and residual strengths were indeed equal in all cases and that the softening rate increased from case B1 through case B3.

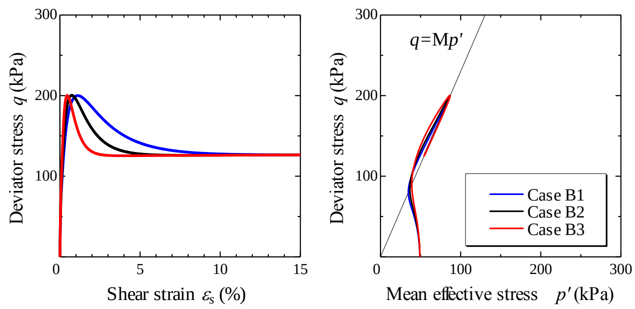

Figure 19 Undrained shear behaviors
(influence of the softening rate from peak to residual state)

Figure 20 shows the load-settlement relationship for these materials and Figure 21 shows the shear strain distributions. From the load-settlement relationship, even when two materials have equal peak strengths on the element level, if they have differing softening rates, it follows that they have different bearing capacities (peak loads). Specifically, the greater the softening rate at the element level, the lower the bearing capacity of the ground, and the degree of load reduction becomes obscure. The reason for this obscurity with increasing softening rate is, as one would expect, that the different elements on the slip lines do not show simultaneous peaks. In other words, when softening is sudden, most of the elements that have already passed their peaks fall to their residual strengths; in comparison to a soil showing gradual softening, there are a limited number of elements undergoing a simultaneous softening process. The shear strain distributions in Figure 21 show that the failure regions have slightly differing sizes, due to the softening rates at the element level, but there is no difference in failure shapes such as is seen when the ratio of residual strength to peak strength is varied. A comparison of Figure 17 and Figure 20 shows that the softening rate has a lower effect on the bearing capacity than the ratio of residual strength to peak strength does.

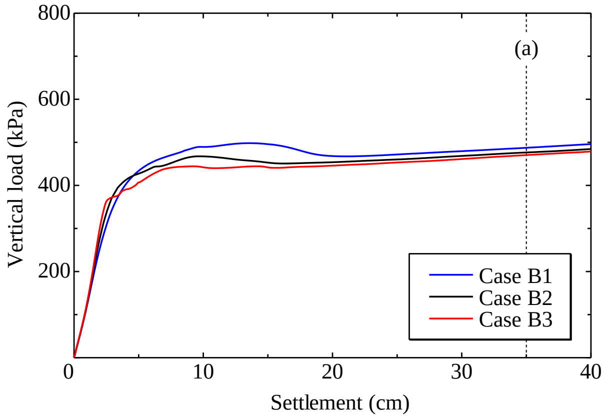

Figure 20 Relation between load and settlement
(influence of the softening rate from peak to residual state)

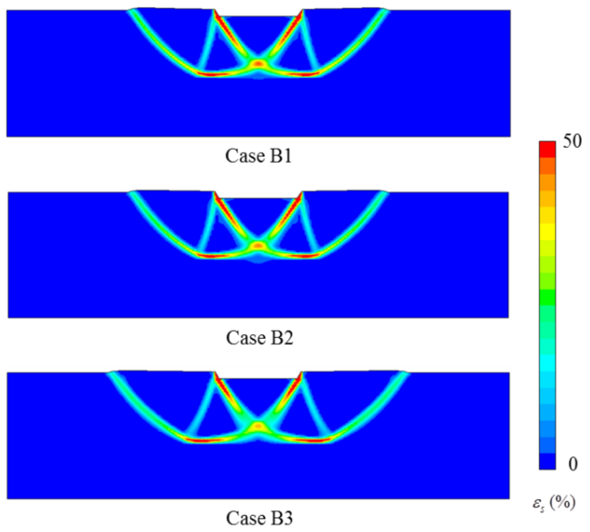

(a) Settlement 35.0cm

Figure 21 Shear strain distributions
(influence of the softening rate from peak to residual state)

5. CONCLUSIONS

In this paper, we investigated the influence of the brittle properties of geomaterials on the failure behavior of ground by means of a numerical method. First, the brittle failure shown by cement treated soil in the undrained triaxial test was reproduced as the softening behavior at the element level using the SYS Cam-clay model, which incorporates the soil skeleton structure at work. Next, undrained bearing capacity analysis of reclaimed ground that has been treated with cement was conducted using the soil-water coupled analysis code ***GEOASIA***, which employs the same constitutive equation. An undrained bearing capacity analysis of naturally deposited clay ground was also selected among past research using the same analysis code for comparison of the failure processes in the two grounds. It was found that even when two soils share the characteristics of a highly developed structure and softening at the element level during undrained shear, they show widely differing failure processes under differing initial conditions. Due to these differing processes, in some grounds, the brittle property of the soil elements do not clearly appear in the bearing capacity characteristics of the ground, while in other grounds, the brittle property do appear. The two typical failure process evident in this study and their characteristics were as follows:

(1) Strain localization in pseudo-overconsolidated ground with uniform void ratio initially occurred directly under the edges of the foundation and the strain localization region then propagated, ultimately forming slip lines in the shape of a circular arc path. Each soil element on the slip lines showed softening behavior sequentially. When progressive failure in which strain localization region develops due to propagation of material failure occurs, even though the ground is composed of brittle materials such as cement treated soil, those brittle properties does not directly manifest in the load-settlement relationship.

(2) The slip lines in ground that are substantively overconsolidated state due to unloading history of surface load suddenly curves into a circular arc shape, after which the strain localization level increases. As this moment, most of the soil elements on the slip lines begin to soften simultaneously, at approximately the same time as the bearing load reaches the peak value. Thus, when failure progresses in this manner, even if the ground composed of ductile materials such as naturally deposited clay, the load reduces clearly as a result.

From the above discussion, it was concluded that individual material properties do not appear straightforwardly on the bearing capacity characteristics of the ground when progressive failure occurs. Based on this finding, a systematic investigation was performed on the influences of the brittle property of the geomaterial on the undrained bearing capacity of the ground, focused on progressive failure. The investigation revealed that, since every soil element on the slip lines does not reach its peak strength simultaneously when progressive failure occurs, post-peak material properties, i.e. the ratio of residual strength to peak strength and the softening rate from peak to residual state have the following effects on the bearing capacity of the ground.

(1) The ratio of residual strength to peak strength of the soil elements affects the bearing capacity (peak load) of the ground. When the elements have identical peak strengths, the lower the residual strength of the geomaterial, the lower the bearing capacity of the ground. The reason the residual strength of the soil elements affects the bearing capacity of the ground is that part of the elements on the slip lines have already reached the residual state or are in the softening state when the peak appears on the load-settlement relationship of the ground. Also, the ratio of residual strength to peak strength of the soil elements affects both the degree of strain localization and the failure mode. The greater the strength reduction, the more clearly defined the shear band, and slip lines close to the shape of a circular arc appears.

(2) The softening rate from peak to residual state of the soil elements affects the bearing capacity (peak load) of the ground. When the elements have identical peak strengths, the greater the softening rate at the element level, the lower the bearing capacity of the ground, and the degree of load reduction becomes obscure. The reason for this is that when the softening rate is high, most of the elements that are past their peak strength subside promptly to their residual strength; there are fewer elements showing simultaneous softening than when the softening rate is low. However, the softening rate has a smaller effect in bearing capacity problems than the ratio of residual strength to peak strength does.

This paper revealed that there is a large variation in the failure processes in bearing capacity problem in accordance with differences of the initial conditions. This paper also demonstrated that when progressive failure occurs, the post-peak soil properties, i.e., the ratio of residual strength to peak strength and the softening rate from peak to residual state, affect the bearing capacity characteristics of the ground. It should be mentioned in closing that we are able to consider these arguments because of the use of an elasto-plastic analysis, which treats failure progressively through deformation. This would, of course, not be possible if a rigid-plastic analysis, which treats only failure, was used.

6. REFERENCES

Asaoka, A., Nakano, M. and Noda, T. (1994): Soil-water coupled behaviour of saturated clay near/at critical state, *Soils and Foundations*, Vol. 34, No. 1, pp. 91-106.

Asaoka, A., Noda, T. and Kaneda, K. (1998): Displacement/traction boundary conditions represented by constraint conditions on velocity field of soil, *Soils and Foundations*, Vol. 38, No. 4, pp. 173-181.

Asaoka, A., Noda, T., Yamada, E., Kaneda, K. and Nakano, M. (2002): An elasto-plastic description of two distinct volume change mechanisms of soils, *Soils and Foundations*, Vol. 42, No. 5, pp. 47-57.

Coastal development institute of technology (2008): Manual of the pneumatic flow mixing method, *Coastal technique library*, No.32, (in Japanese).

Kasama, K., Andrew, J., W. and Zen., K. (2012): Effect of spatial variability on the bearing capacity of cement-treated ground, *Soils and Foundations*, Vol. 52, No. 4, pp. 600-619.

Mitarai, Y., Yasuhara, K., Kikuchi, Y. and Karmokar., K., A. (2007): Development of cement treated clay mixed with scrap tire chips as novel geomaterial and study of its mechanical properties, Journal of JSCE C, Vol.63, No.3, pp.881-900, (in Japanese).

Nakano, M. Nakai, K. Noda, T. and Asaoka, A. (2005): Simulation of shear and one-dimensional compression behavior of naturally deposited clays by Super/subloading Yield Surface Cam-clay model, *Soils and Foundations*, Vol.45, No.1, pp.141-151.

Noda, T., Yamada, S. and Asaoka, A. (2005): Elasto-plastic behavior of naturally deposited clay during/after sampling, *Soils and Foundations*, Vol. 45, No. 1, pp. 51-64.

Noda, T., Asaoka, A. and Yamada, S. (2007a): Some bearing capacity characteristics of a structured naturally deposited clay soil, *Soils and Foundations*, Vol. 47, No. 2, pp. 285-301.

Noda, T., Asaoka, A., Nakai, K. and Tashiro, M. (2007b): Structural upgradation in clay and sand accompanying plastic swelling, *Proc. of the13th Asian regional conference on soil mechanics and geotechnical engineering*, pp. 23-26.

Noda, T., Asaoka, A. and Nakano, M. (2008): Soil-water coupled finite deformation analysis based on a rate-type equation of motion incorporating the SYS Cam-slay model, *Soils and Foundations*, Vol. 48, No. 6, pp. 771-790.

Oda, M., Koishikawa, I. and Higuchi, T. (1978): Experimental study of anisotropic shear strength of sand by plane strain test, *Soils and Foundations*, Vol. 18, No. 1, pp. 25-38.

Oda, M. and Koishikawa, I. (1979): Effect of strength anisotropy in bearing capacity of shallow footing in a dense sand, *Soils and Foundations*, Vol. 19, No. 3, pp. 15-28.

Tashiro, M., Noda, T. and Nakano, M. (2004): Astudy on “pseudo-overconsolidation effect” of clay in terms of active soil structure, *Journal of applied mechanics JSCE*, Vol. 7, pp. 589-596, (in Japanese).

Tatsuoka, F. (1992): Easy to understand soil mechanics theory—taking as an example the problem of bearing capacity of a foundation on a sandy ground—relationships among laboratory shear tests, in-situ geotechnical investigations, stability analysis, model testing, and the actual behavior of a real structure (1st revision), *Japanese Geotechnical Society*, pp. 109-154, (in Japanese).

Tatsuoka, F. (2007): Design shear strength and compaction control of backfill a current wide and deep gap between industry and academia, *Proc. of the13th Asian regional conference on soil mechanics and geotechnical engineering*, Vol. 2, pp. 442-451, (in Japanese).

Tsukiji, K., Ochiai, H., Yasufuku, N., Omine, K. and Miyazaki Y. (1998): Effective usage of plastic waste focused on strength improvement effect of cement treated soil, *Proc. of the 3rd symposium on ground improvement*, pp.169-176, (in Japanese).

Yamamoto, M., Izutsu, T., Terashi, M. and Ishii, T. (2006): The bearing capacity characteristics of the low-strength and uniformly-improved ground, *Proc. of the 59th Annual Conference of JSCE*, pp.1029-1030, (inJapanese) .